Journal of Alloys and Compounds 509 (2011) 5414–5419

Contents lists available at ScienceDirect

Journal of Alloys and Compounds

journal homepage: www.elsevier.com/locate/jallcom

Catalyst-free synthesis, morphology evaluation and photocatalytic properties of pristine and calcinated titanate nanorods

Beata Zielińska*, Ewa Borowiak-Palen, Barbara Grzmil, Ryszard J. Kalenczuk

Institute of Chemical and Environment Engineering, West Pomeranian University of Technology, Szczecin Pułaskiego 10, 70-322 Szczecin, Poland

ARTICLE INFO

Article history:
Received 2 June 2010
Received in revised form 10 February 2011
Accepted 15 February 2011
Available online 22 February 2011

Keywords:
Nanostructured materials
Chemical synthesis
Catalysis
Optical properties

ABSTRACT

Titanate nanorods with high photocatalytic activity was successfully synthesized through a simple catalyst-free hydrothermal method. The photocatalytic degradation of a model organic dye (Reactive Red 198) was accelerated by the calcination of the nanorods prior the reaction. The calcination of nanorods did not modify their morphology, however the crystallinity of the samples was significantly improved. Therefore, the quality of the samples is a key parameter determining their activity in the investigated photocatalytic process. The as-produced and annealed catalysts were characterized by high-resolution transmission electron microscopy (HR-TEM), X-ray diffraction (XRD), Diffuse Reflectance (DR) UV–Vis and resonance Raman spectroscopy.

1. Introduction

In the past decades, one-dimensional (1-D) nanostructures have received significant attention due to their remarkable electronic, magnetic, optical, catalytic and mechanical properties and potential applications in nanodevices [1–4]. Among the various oxide and non-oxide 1-D nanostructured materials, titanate nanostructures (nanotubes, nanorods, nanowires, nanoribbons and whiskers) have received great attention due to their wide application in photovoltaic cells, photocatalysis, catalytic supports and gas sensors [1,5–8]. Various methods for the preparation of 1-D titanate nanomaterials such as combining sol–gel processing, sonochemical synthesis and pyrolysis route are used [9–11]. Nevertheless, one of the most promising synthesis of those nanomaterials is hydrothermal treatment of titania powder containing different crystallography (rutile, anatase and brookite) in a strong aqueous solution of NaOH or KOH. Kasuga et al. (1998–1999) [12] prepared TiO_2-derived nanotubes with diameter of about 8 nm using this technique. The main advantages of this method are its simplicity, reproducibility and no need to use the catalysts. Therefore, there is no issue with sample purification after the preparation what is widely studied e.g. in case of carbon nanotubes synthesis [13].

The photocatalytic activity of titanate nanostructured materials has been intensively studied by many researches [1,5–8,14]. For example, S. Mozia et al. [14] reported that titanate nanotubes (TNTs), produced via hydrothermal method, exhibited no photoactivity toward degradation of model azo dye (Acid Red 18). However, they stated that TNTs have been successfully applied in photocatalytic generation of CH_4 and H_2 in a solution of acetic acid. H. S. Hafez [15] produced single-crystalline anatase TiO_2 nanorods via a two-step, hydrothermal treatment of anatase/rutile TiO_2 powder and acid-post treatment. The photocatalytic performance of the prepared nanorods was tested in the photocatalytic degradation of the commercial Ciabacrown Red textile dye under UV illumination. Authors indicated that anatase TiO_2 nanorods are highly active in the dye removal. J. Yu et al. [8] obtained mesoporous anatase TiO_2 nanofibres with high photocatalytic activity by hydrothermal post-treatment of titanate nanotubes. The annealing of titanate tubes at 200 °C resulted in the destruction of nanotubular structure and the formation of anatase TiO_2 nanofibres. They reported that the photocatalytic activity of TiO_2 nanofibres exceeded that of Degussa P25.

In the present work, titanate nanorods were prepared via a hydrothermal treatment of titanium dioxide (TiO_2-Degussa P25) in 10 M NaOH solution at 210 °C for 24 h, followed by washing with HCl solution and distilled water. The effect of calcination of as-produced nanorods on their morphology was investigated. Finally, the photocatalytic activity of as-produced and calcinated photocatalysts was evaluated. As a model reaction the photocatalytic decolourization of organic dye RR198 (Reactive Red 198) was applied.

2. Experimental

2.1. Materials

Commercial TiO_2-P25 (Degussa P25, Germany) with crystalline structure of ca. 80% anatase and ca. 20% of rutile and sodium hydroxide (Aldrich) were used for

* Corresponding author. Tel.: +48 91 449 43 97; fax: +48 91 449 46 86.
E-mail address: bzielinska@zut.edu.pl (B. Zielińska).

0925-8388/$ – see front matter © 2011 Elsevier B.V. All rights reserved.
doi:10.1016/j.jallcom.2011.02.069

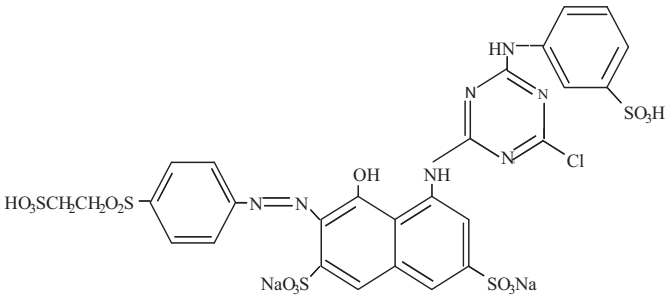

Fig. 1. The molecular formula of Reactive Red 198.

the synthesis of titanate nanorods. Reactive Red 198 (RR198) produced by "Boruta Color" company (Poland) was selected as a model contaminant. The photocatalytic decolourization of RR198 solution over produced catalysts will be investigated. RR198 is a water-soluble azo-dye with molecular formula presented in Fig. 1.

2.2. Preparation of titanate nanomaterials

Titanate nanorods were hydrothermally synthesized as follows: 2 g of TiO_2-P25 was added to 50 cm^3 of aqueous solution of 10 M NaOH. This was poured into teflon-lined stainless steel with a capacity of 70 cm^3. The sealed autoclave was heated to 210 °C and maintained at this temperature for 24 h. The final product was collected by filtration and washed with 0.1 M HCl (to eliminate sodium ions incorporated in the structure). Afterwards it was re-dispersed with the assistance of ultrasounds. Now sample was washed again with distilled water until the pH of supernatant reached 7, and finally dried in air at 70 °C for 24 h. The sample prepared in the above-described way will be labeled as S. Finally the sample S was divided into three equal batches and each of the batch was calcinated at 400 °C, 500 °C and 600 °C in air for 3 h, respectively. The calcinated materials will labeled as **ST** (T means the temperature of calcination).

2.3. Experimental procedure and techniques

The morphology and chemical composition of the prepared samples were examined using a high-resolution transmission electron microscopy (HR-TEM-FEI Tecnai F30) and energy dispersive X-Ray spectrometer (EDX) as its mode. The crystallographic structure of the samples were characterized by X-ray diffraction (XRD) analysis (X'Pert PRO Philips diffractometer) using a CuK_α radiation. The optical properties of the materials were investigated by means of Diffuse Reflectance (DR) UV–Vis technique using Jasco (Japan) spectrophotometer. Additionally, resonance Raman study was performed using resonance Raman Renishaw InVia Microscope with laser length 785 nm.

2.4. Determination of photocatalytic activity

The photocatalytic activity of the as-prepared (**S**) and annealed (**ST**) was examined in the reaction of the photocatalytic decolourization of the organic dye. The photocatalytic reaction was carried out in an open glass reactor containing 20 cm^3 of a model solution of RR198 (initial concentration-30 mg/dm^3) and 10 mg of the catalyst. Firstly, the mixture was suspended in the ultrasonic bath for 0.5 h. Afterwards, the solution was irradiated using 60 W lamp. Next, it was filtered through a 0.45 μm membrane filter. The evaluation of the dye concentration was performed by means of UV–Vis spectrophotometer (Jasco V-530, Japan) at fixed wavelengths of 518 nm (RR198).

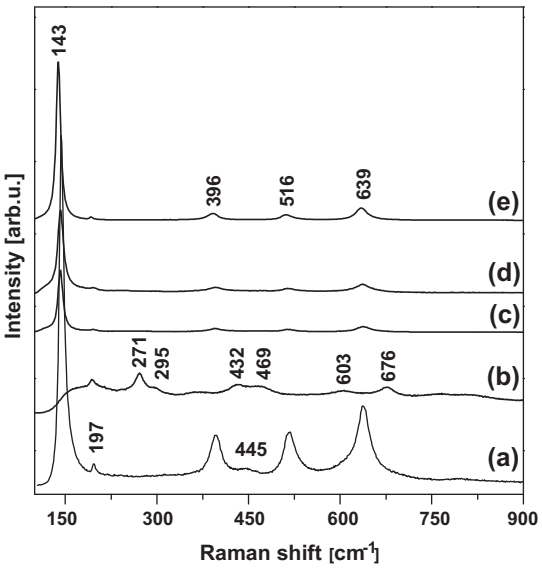

Fig. 3. Raman spectra of samples: (a) TiO_2-P25, (b) **S**, (c) **S400**, (d) **S500** and (e) **S600**.

3. Results and discussion

The crystal structure of the starting material TiO_2-P25 (pattern a), nanorods (**S**-pattern b) and calcinated nanorods at 400 °C, 500 °C and 600 °C (**S400**, **S500** and **S600**-patterns-c–e) were identified by XRD as shown in Fig. 2. TiO_2-P25 is a mixture of anatase (JCPDS card no. 21-1272) and rutile (JCPDS card no. 34-180). The detailed phase analysis of the sample **S** (pattern b) revealed that it was a mixture of sodium titanate (Na_2TiO_3, JCPDS card no. 00-011-0291) and hydrogen pentatitanate ($H_2Ti_5O_{11}\cdot H_2O$, JCPDS card no. 00-044-0131). It means that the sodium ions removal from the sample S was not fully efficient and sodium in the form of Na_2TiO_3 remained in the sample **S**. Moreover, Fig. 2 shows that the samples **S400** and **S500** are composed of TiO_2 (B) (JCPDS card no. 00-046-1238). TiO_2 (B) is metastable polymorph titanium dioxide formed by the dehydration of layer or tunnel structured hydrogen titanate (it is also named as

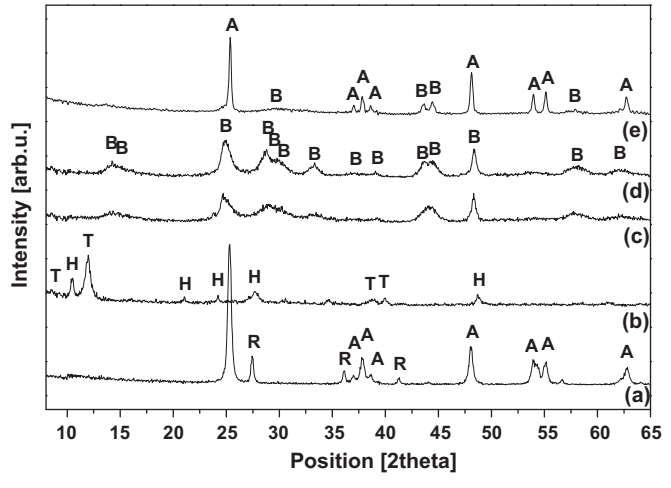

Fig. 2. XRD patterns of TiO_2-P25 (a), **S** (b), **S400** (c), **S500** (e) and **S600** (f) (A-anatase, R-rutile, B-TiO_2 (B), T–Na_2TiO_3 and H–$H_2Ti_5O_{11}\cdot H_2O$).

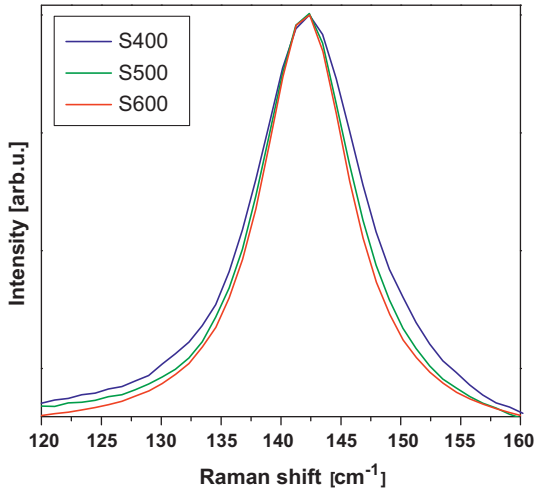

Fig. 4. Normalized Raman spectra of the **S400**, **S500** and **S600** samples at 142 cm^{-1}.

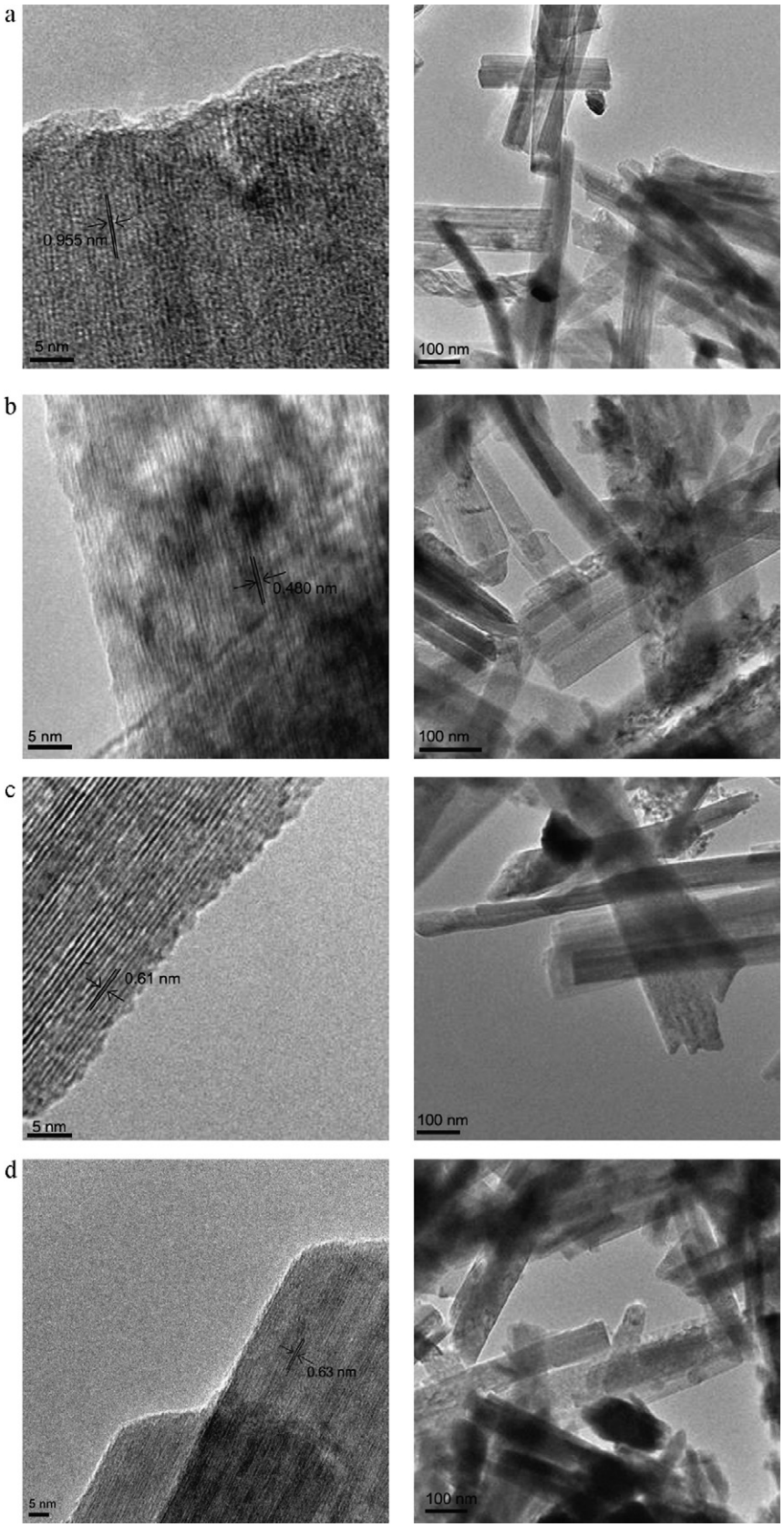

Fig. 5. TEM images of **S** (a), **S400** (b), **S500** (c) and **S600** (d) samples.

monoclinic TiO_2) [16]. The increase of the calcination temperature to 600 °C (**S600**) led to the appearance of anatase phase as a main phase, but the diffraction peaks of TiO_2 (B) were simultaneously detected. Here, the puzzling is that the sodium titanate phase was not detected in XRD patterns of **S400**, **S500** and **S600**. This means that sodium could evaporate during the calcination process. It was already reported that the annealing could change the phase composition of the sample e.g. X. Zhang et al. [17] observed that the protonated titanate ($H_2Ti_2O_5$) was fully dehydrated and converted into TiO_2 (B) phase at temperature of 500 °C and into anatase phase at 600 °C. W. Li et al. [18] suggested that annealing of $H_2Ti_5O_{11}$ favored the formation of a TiO_2 (B) structure, whereas $H_2Ti_2O_5$ underwent the transition into anatase. Moreover, Z.-Y. Yuan [19] reported that $H_2Ti_5O_{11}{\cdot}H_2O$ was completely dehydrated and recrystallized into TiO_2 (B) in the temperature range of 400–600 °C. In the temperature range of 700–900 °C, the metastable TiO_2 was transformed into anatase, which was then changed into rutile phase.

Fig. 3 shows the resonance Raman spectra of the pristine TiO_2-P25 (spectrum a), and the produced samples (spectra b–e). In this figure it is clearly seen that the spectrum of the TiO_2-P25 shows six peaks: at ~142 cm^{-1}; 191 cm^{-1}; 396 cm^{-1}; and 445 cm^{-1} of very weak intensities, and well pronounced bands at 516 cm^{-1} and 639 cm^{-1}. Five of those peaks (142 cm^{-1}; 191 cm^{-1}; 396 cm^{-1}; 516 cm^{-1}; and 639 cm^{-1}) are assigned to anatase phase while one peak (445 cm^{-1}) corresponds to rutile [20,21]. In the case of the sample **S** (spectra b) the bands at ~197 cm^{-1}, 271 cm^{-1}, 432 cm^{-1}, 469 cm^{-1}, 603 cm^{-1} and 676 cm^{-1} are observed. The Raman modes at about 198 cm^{-1}, and in the region of 224–339 cm^{-1} (~271 cm^{-1}) are assigned to the stretching mode of Ti–O–Na [9]. The bands at 469 cm^{-1} and 603 cm^{-1} correspond to the bending and stretching vibrations of Ti–O bonds, respectively. The band at 676 cm^{-1} is attributed to Ti–O–Ti stretching vibrations [22]. Raman peaks in the region of 224–339 cm^{-1} corresponding to the Ti–O–Na stretching vibration in all annealed samples are not detected. This clearly indicates the absence of sodium ions in the **S400**, **S500** and **S600** nanorods. This is in agreement with XRD analysis. Raman spectra of the calcinated samples (**S400**, **S500**, and **S600**) show five peaks at 142 cm^{-1}, 191 cm^{-1}, 396 cm^{-1}, 516 cm^{-1} and 639 cm^{-1} which are characteristic for anatase phase of TiO_2. The tendency of the intensity enhancement of all the bands corresponding to anatase with the temperature increase is detected. The normalized Raman spectra of samples **S400**, **S500** and **S600** at 142 cm^{-1} are presented in Fig. 4. Here, the increase of the calcination temperature results in the narrowing of the width at half of the maximum intensity (FWHM) of this peak. The increase of the intensity of the peaks, and the decrease of FWHM can be attributed to the improvement in the crystallinity of the annealed samples [23,24].

The morphology and chemical composition of the samples were studied using HR-TEM and EDX as its mode. The TEM images of the samples **S**, **S400**, **S500** and **S600** are presented in Fig. 5. Fig. 6 shows the histograms of the rods diameter distribution in the samples. The sample S consists of nanorod particles with diameter in the range of 18–50 nm. The samples **S400**, **S500**, and **S600** show a rod-like morphology similar to the starting sample **S**. However, the diameter distribution of the nanorods of the calcinated samples gradually broadened upon the thermal treatment. The samples **S400**, **S500**, **S600** are composed of nanorods with the diameter distribution in the range of 30–90 nm, 25–90 nm and 22–90 nm, respectively. The diameter distribution of the heated samples increases by the factor of two in respect to the starting material (**S**). This can be explained by the fact that the annealing step changes the phase composition of the samples what was described in the previous section. The sodium titanates underwent decomposition to Na and probably to TiO_2. Those TiO_2 fraction of the sample could become a part of already existing TiO_2 rods and therefore responsible for the sample

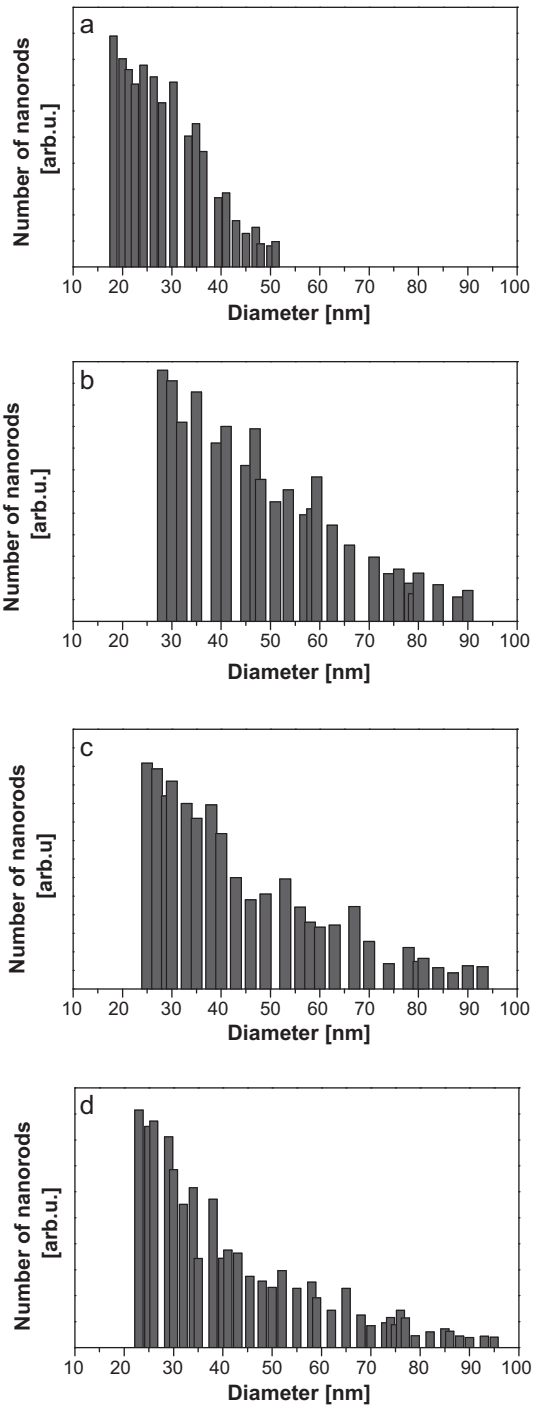

Fig. 6. Histograms presenting the diameter distribution of nanorods: (a) **S**, (b) **S400**, (c) **S500** and (d) **S600**.

diameter distribution broadening. H. Yu et al. [1] studied the influence of calcination temperature (temperature range of 300–900 °C) on the structure of H-titanate nanowires and noticed the increase of nanorods diameter in the samples calcinated above 600 °C. Even, the presence of nanorods with diameter over 200 nm at 900 °C has been observed. In our contribution the calcination of sample **S** at temperature range between 400 °C and 600 °C did not result in the modification of the length of the produced nanorods. The length of the nanorods ranged from ~100 nm to several μm for all produced nanorods (**S**, **S400**, **S500**, and **S600**). Moreover, it is noticed that **S**, **S400**, **S500**, **S600** nanorods exhibit well crystallized layered struc-

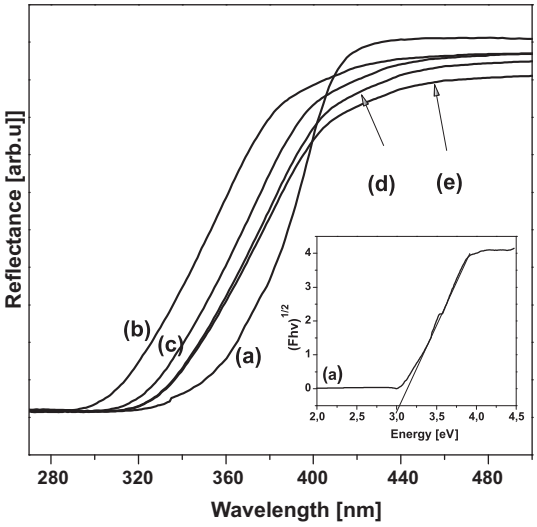

Fig. 7. UV–vis diffuse reflectance spectra of (a) TiO_2-P25, (b) **S**, (c) **S400**, (d) **S500** and (e) **S600** (The inset-Kubelka–Munk plot for band gap evaluation of TiO_2-P25 sample).

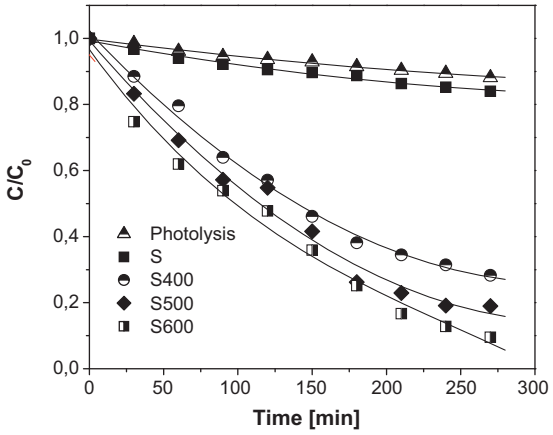

Fig. 8. Photocatalytic decolourization of RR198 in the presence of **S**, **S400**, **S500** and **S600** samples.

ture. Sample **S** has a layer spacing of 0.96 nm. The layer spacing of the calcinated samples was getting lower in respect to the sample **S**. The decrease of the layer spacing of the calcined nanorods can be attributed to the phase transformation from Na_2TiO_3 and $H_2Ti_5O_{11}{\cdot}H_2O$ (**S**) to TiO_2 (B) and anatase (**ST**). This can be explained by the effect of dehydration of the $H_2Ti_5O_{11}{\cdot}H_2O$ during the calcination. The layer spacing of **S400**, **S500** and **S600** is about 0.48 nm, 0.61 nm and 0.63 nm, respectively. In general, the increase of the calcination temperature expands the interlayer spacing in the crystal structure of nanorods, but does not reach the value of the sample **S**.

Table 1 presents quantitative analysis of EDX spectra of the samples. **S400**, **S500** and **S600** demonstrated the absence of sodium in the nanorods. Those samples are composed only of oxygen and titanium. This results is in agreement with XRD and Raman analysis. Only in sample **S** sodium was detected. Moreover, the quantitative analysis gave an approximate Ti:O weight ratio of 58:42, 59:41 and 59:41 for **S400**, **S500** and **S600**, respectively. It is very close to the ratio of TiO_2 (60:40).

In order to estimate the band gap of the samples the optical analysis was conducted. Fig. 7 presents the DR-UV–vis spectra of pristine TiO_2-P25 (spectrum a), and samples **S**, **S400**, **S500**, **S600** (spectra b–e). A UV–vis absorption reflects the gap between the valence and conduction band of the studied samples. Here in each spectrum of all the samples a single UV absorption edge is detected. These absorption edges shifted toward the shorter wavelength in comparison to the pristine TiO_2-P25. This indicates the increase of the band gap energy. To determine their band gaps, the Kubelka–Munk method based on the diffuse reflectance spectra was employed. The gap energy of the samples can be estimated from a plot of $(F(R)h\nu)^{1/2}$ versus photon energy ($h\nu$), where $F(R) = (1 - R)/2R$ ($F(R)$ is the Kubelka–Munk function, R-reflectance)

Table 1
EDX quantitative analysis of the **S**, **S400**, **S500**, **S600** samples.

Sample	Elemental weight (%)		
	O	Ti	Na
S	40.13	56.45	3.43
S400	41.55	58.44	X
S500	40.68	59.32	X
S600	41.03	58.97	X

[14,23]. For example, the inset in Fig. 7 shows the plot of $(F(R)h\nu)^{1/2}$ versus photon energy ($h\nu$) for TiO_2-P25. The estimated band gap energy of TiO_2-P25 is equal 3.05 eV (This is the same as previously described in the literature [25,26]). It was calculated that the produced nanorods (**S**) had band gap energy of 3.42 eV which is larger than the TiO_2-P25. It was also observed by H. Jia et al. [27]. Moreover, the calcination of nanorods in the temperature range of 400–600 °C caused the decrease of their band gaps in respect to sample **S**. The band gap energy of **S400**, **S500** and **S600** is about 0.06 (3.36 eV), 0.21 (3.21 eV) and 0.24 eV (3.18 eV) lower than that of nanorods S, respectively. Additionally, the band gap of **S600** is close to the band gap value of anatase. It stands from fact that the **S600** contains the anatase phase of TiO_2 (as a main phase) and small fraction of TiO_2 (B). It is well known that the band gap energy of anatase is equal 3.2 eV [28–30]. The band gap of TiO_2 (B) (**S400** and **S500**) is larger than that of anatase. This results is in agreement with previous reports [1,31].

Finally, the photocatalytic activity of the produced materials (**S**, **S400**, **S500** and **S600**) has been tested in the decolourization reaction of a model organic dye (RR198-Reactive Red 198). Reactive red 198 was already investigated using TiO_2 powder [32]. In order to determine the photostability of investigated azo-dye (RR198) a photolysis experiment (i.e. without addition of photocatalysts) was performed. The comparison of RR198 decolourization with and without studied photocatalysts is presented in Fig. 8. This figure shows a plot of C/C_0 versus time (t), where C is concentration of the dye at the certain time and C_0 is initial concentration of dye (mg/dm^3). The as-prepared nanorods (S) exhibit low photocatalytic activity in the studied reaction. This activity is close to the photolysis of RR198. However, the annealed nanorods significantly accelerated its decolourisation. This could be attributed to the enhancement of the samples crystallinity (quality) upon the annealing. This means that the improved crystallinity of the catalysts is a key factor improving their photocatalytic activity. This could be due to the fact that the number of defect sites, regarded as a major pathway of the recombination between photogenerated electrons and holes, could be reduced, and the space change separation become more efficient [33]. Moreover, the sample **S600**, which shows the highest photoactivity, is composed of two crystal phases, such as anatase and TiO_2 (B). Therefore, the highest photocatalytic activity of **S600** can be explained by two effects: (i) improved crystallinity and (ii) the phase composition which might be advantageous in the separation of photogenerated electrons and holes reducing the recombination [18,34]. W. Li et al. [18] stated that TiO_2 (B) possesses higher valence (CV) and conduction (CB) bands edge potential than anatase. Therefore, the holes generated in anatase

would migrate toward the TiO_2 (B) phase because of the higher valence band (VB) edge potential. While, the photoinduced electrons in the conduction band of TiO_2 (B) could favor migration to the anatase phase exhibiting lower conduction band potential [18]. In our case, when the band gap energy of the calcinated nanorods decreased the photocatalytic activity of the calcinated nanorods increased. It means that the lower band gap energy allows lower energy photons to excite electron-hole pairs, which then can react with adsorbed molecules.

As described in the introduction section, the photocatalytic activity of different nanostructured materials has been intensively studied [1,5–8,14,15,27,35,36]. Many researches [1,14,35,36] indicated that nanorods and nanotubes produced in the hydrothermal reaction exhibited no photocatalytic activities. It was also described that photocatalytic activity of those structures strongly depend on the calcination temperature [1,35,36] what is also shown in our study. For example, H. Yu [1] and J. Yu [35] et al. studied photocatalytic oxidation of acetone in the presence of calcinated H-titanate nanowires and titanate nanotubes. It is interesting that authors obtained the similar relationships for both kinds of investigated nanostructures (nanowires and nanotubes). They found that as-prepared nanowires and nanotubes showed no photocatalytic activities in the above mentioned reaction. They also state that the calcinated nanomaterials exhibited higher activities than as-prepared samples. For the calcination temperature lower than 400 °C, the produced nanowires and nanotubes did not show any activities. When the calcination temperature increased to 500 °C, their photoactivity also increased. Further increase of the calcination temperature (600–800 °C) caused the decrease of the sample activities. M. Qamar et al. [36] studied the photocatalytic activity of titanate nanotubes in the reaction of photooxidation of amaranth as a function of sodium content and the calcination temperature. They also found that as-prepared nanotubes, with and without sodium content exhibited no photocatalytic activity. However, the photocatalytic activity of the nanotubes drastically increased after calcination of the sample prior the reaction.

Therefore the annealing of the candidates as photocatalysts seems to be a crucial to determine their activity. This indicates that to evaluate the photocatalytic activity of the catalyst the systematic study with the annealed material should be also performed. This clearly could expand specialized and industrial applications of the nanostructured TiO_2 materials.

4. Conclusions

In summary, titanate nanorods (**S**) with a diameters of about 18–50 nm and layer spacing of 0.96 nm were synthesized via the hydrothermal reaction of TiO_2–Degussa P25 and NaOH solution in the temperature of 210 °C. The effect of calcination temperature (400–600 °C) on morphology and photocatalytic activity of the as-produced nanorods were investigated. Here we proved that the diameter distribution of the calcinated nanorods broadened in comparison to the as-prepared material. Moreover, the calcination of as-produced nanorods lead to the significant enhancement of the photocatalytic efficiency of this materials in the decolourization of RR198. Therefore, the calcination step is crucial in order to enhance the photocatalytic activity of nanorods.

References

[1] H. Yu, J. Yu, B. Cheng, Chemosphere 66 (2007) 2050–2057.
[2] T. Kasuga, M. Hiramatsu, A. Hoson, et al., Langmuir 14 (1998) 3160–3163.
[3] H. Yu, J. Yu, B. Cheng, et al., J. Solid State Chem. 179 (2006) 349–354.
[4] D. Wu, J. Liu, X. Zhao, et al., Chem. Mater. 18 (2006) 547–553.
[5] J. Yu, Q. Xiang, M. Zhou, Appl. Catal. B 90 (2009) 593–602.
[6] H. Yu, J. Yu, B. Cheng, J. Lin, J. Hazard. Mater. 147 (2007) 581–587.
[7] X. Bai, B. Xie, N. Pan, X. Wang, H. Wang, J. Solid State Chem. 181 (2008) 450–456.
[8] J. Yu, H. Yu, B. Cheng, X. Zhao, Q. Zhang, J. Photochem. Photobiol. A 182 (2006) 121–127.
[9] Y.V. Kolen'ko, K.A. Kovnir, A.I. Gavrilov, et al., J. Phys. Chem. B 110 (2006) 4030–4038.
[10] C. Xu, Y. Zhan, K. Hong, Solid State Commun. 126 (2003) 545–549.
[11] Y. Zhu, H. Li, Y. Koltypin, Y.R. Hacohen, A. Gedanken, Chem. Commun. 24 (2001) 2616–2617.
[12] T. Kasuga, M. Hiramatsu, A. Hoson, et al., Adv. Mater. 11 (1999) 1307–1311.
[13] J.-F. Colomer, P. Piedigrosso, A. Fonseca, J.B. Nagy, Synthetic Met. 103 (1999) 2482–2483.
[14] S. Mozia, E. Borowiak-Paleń, J. Przepiórski, et al., J. Phys. Chem. Solids 71 (2010) 263–272.
[15] H.S. Hafez, Mater. Lett. 63 (2009) 1471–1474.
[16] A.J. Jitputti, Y. Suzuki, s. Yoshikawa, Catal. Commun. 9 (2008) 1265–1271.
[17] X. Zhang, J.H. Pan, A.J. Du, J. Ng, D.D. Sun, J.O. Leckie, Mater. Res. Bull. 44 (2009) 1070–1076.
[18] W. Li, Ch. Liu, Y. Zhou, Y. Bai, X. Feng, Z. Yang, L. Lu, X. Lu, K.-Y. Chan, J. Phys. Chem. C 112 (2008) 20539–20545.
[19] Z.Y. Yuan, B.-L. Su, Colloid Surf. A 241 (2004) 173–183.
[20] R Ma, K. Fukuda, T. Sasaki, M. Osada, Y. Bando, J. Phys. Chem. B 109 (2005) 6210–6214.
[21] L. Qian, Z.-L. Du, S.-Y. Yang, Z.-S. Jin, J. Mol. Struct. 749 (2005) 103–107.
[22] X. Meng, D. Wang, J. Liu, S. Zhang, Mater. Res. Bull. 39 (2004) 2163–2170.
[23] Y. Sua, J. Yua, J. Lin, J. Solid State Chem. 180 (2007) 2080–2087.
[24] B. Karunagaran, K. Kim, D. Mangalaraj, J. Yi, S. Velumani, Sol. Energy Mater. Sol. C 88 (2005) 199–208.
[25] M.A. Khan, M.S. Akhtar, S.I. Woo, O.-B. Yang, Catal. Commun. 10 (2008) 1–5.
[26] J. Zhou, M. Takeuchi, A.K. Ray, M. Anpo, X.S. Zhao, J. Colloid Interface Sci. 311 (2007) 497–501.
[27] H. Jia, Z. Zheng, H. Zhao, L. Zhang, Z. Zou, Mater. Res. Bull. 44 (2009) 1312–1316.
[28] R. Long, Y. Dai, B. Huang, Comp. Mater. Sci. 45 (2009) 223–228.
[29] L. Wan, J.F. Li, J.Y. Feng, W. Sunb, Z.Q. Mao, Mater. Sci. Eng. B 139 (2007) 216–220.
[30] A.V. Murugan, V. Samuel, V. Ravi, Mater. Lett. 60 (2006) 479–480.
[31] A. Yin, J. Wu, M. Aki, T. Sato, Int. J. Inorg. Mater. 2 (2000) 325–331.
[32] S. Dutta, S.A. Parsons, C. Bhattacharejee, P. Jarvis, S. Datta, S. Bandyopadhyay, Chem. Eng. J. 155 (2009) 674–679.
[33] A.-K. Chakraborty, z. Qi, S.-Y. chai, Ch. Lee, S.-Y. Park, D.-J. Jang, W.-I. Lee, Appl. Catal. B 93 (2010) 368–375.
[34] J. Zhu, J. Zhang, F. Chen, M. Anpo, Mater. Lett. 59 (2005) 3378–3381.
[35] J. Yu, H. Yu, B. Cheng, C. Trapalis, J. Mol. Catal. A 249 (2006) 135–142.
[36] M. Qamar, C.R. Yoon, H.J. Oh, et al., Catal. Today 131 (2008) 3–14.